

Xuepu Wang | Marcel Sperling | Martin Reifarth | Alexander Böker

Shaping Metallic Nanolattices: Design by Microcontact Printing from Wrinkled Stamps

Suggested citation referring to the original publication:

Small 16 (2020) 11, Art. 1906721 pp. 1 - 8

DOI <https://doi.org/10.1002/sml.201906721>

ISSN 1613-6810, 1613-6829

Journal article | Version of record

Secondary publication archived on the Publication Server of the University of Potsdam:

Zweitveröffentlichungen der Universität Potsdam : Mathematisch-Naturwissenschaftliche Reihe 1391

ISSN: 1866-8372

<https://nbn-resolving.org/urn:nbn:de:koby:517-opus4-514341>

DOI: <https://doi.org/10.25932/publishup-51434>

Terms of use:

This work is licensed under a Creative Commons License. This does not apply to quoted content from other authors. To view a copy of this license visit

<https://creativecommons.org/licenses/by/4.0/>.

Shaping Metallic Nanolattices: Design by Microcontact Printing from Wrinkled Stamps

Xuepu Wang, Marcel Sperling, Martin Reifarth, and Alexander Böker*

A method for the fabrication of well-defined metallic nanostructures is presented here in a simple and straightforward fashion. As an alternative to lithographic techniques, this routine employs microcontact printing utilizing wrinkled stamps, which are prepared from polydimethylsiloxane (PDMS), and includes the formation of hydrophobic stripe patterns on a substrate via the transfer of oligomeric PDMS. Subsequent backfilling of the interspaces between these stripes with a hydroxyl-functional poly(2-vinyl pyridine) then provides the basic pattern for the deposition of citrate-stabilized gold nanoparticles promoted by electrostatic interaction. The resulting metallic nanostripes can be further customized by peeling off particles in a second microcontact printing step, which employs poly(ethylene imine) surface-decorated wrinkled stamps, to form nanolattices. Due to the independent adjustability of the period dimensions of the wrinkled stamps and stamp orientation with respect to the substrate, particle arrays on the (sub)micro-scale with various kinds of geometries are accessible in a straightforward fashion. This work provides an alternative, cost-effective, and scalable surface-patterning technique to fabricate nanolattice structures applicable to multiple types of functional nanoparticles. Being a top-down method, this process could be readily implemented into, e.g., the fabrication of optical and sensing devices on a large scale.

optoelectronics.^[12–14] Thereby, templating by surface patterns represents a popular method to obtain fine metallic nanostructures. Different types of advanced lithographic techniques have been utilized to fabricate functional surface patterns, such as photo-,^[15,16] electron-beam or dip-pen lithography,^[6,17–20] self-assembly patterns (SAPs) of (macro-)molecules,^[21–24] soft lithography and others.^[25–27] Photo- or non-photo lithography as well as dip-pen lithography, however, require specialized and expensive equipment, which drastically limits their applicability. The preparation of SAPs is difficult to be scaled up over large areas or volumes. On the contrary, soft lithography, which is a combination of SAPs and large-area surface patterning, constitutes a more convenient method. As such, microcontact printing (μ CP), as the most prominent variation of soft lithography, represents a cheap and straightforward method that does not require sophisticated instrumentation.^[28,29]

An excellently suited material for soft lithography is the elastomer polydimethylsiloxane (PDMS). PDMS can be surface-structured in a straightforward and inexpensive fashion into (sub-)micrometer-sized regular patterns by plasma-induced surface wrinkling.^[30–33] These patterns can be used to guide particle assembly, thereby avoiding the utilization of expensive masters, which are usually fabricated by the already mentioned methods of photo or non-photo lithography. In recent years, PDMS wrinkle templates have been widely used to directly assemble organic^[34–36] and inorganic particles^[37–39] as well as biomaterials,^[40,41] which led to functional nano- or micro-structures applicable for, e.g., plasmonics,^[37–39] or wetting switches.^[42] Nevertheless, up to now there are only a limited number of studies about chemical patterns fabricated by using PDMS wrinkles to guide self-assembly of particles.


Motivated by the ease and adjustability of their preparation, we developed a fast and feasible method for chemical patterning based on μ CP via the utilization of wrinkled PDMS. Our aim was to take advantage of the oligomeric PDMS, which is inherently present within cured PDMS and usually represents a nuisance for μ CP, and turn it into a useful tool for the preparation of sophisticated surface patterns on the micro- to nanoscale. This led us to a consecutive routine, which consists of few easy-to-apply preparation steps yielding nanoparticulate patterns of different adjustable geometries with high regularity. Hence, this work contributes to the effort of improving the applicability of surface patterning by reducing cost, which may

1. Introduction

Structured metallic nanoparticle assemblies, particularly if fabricated with a high degree of specificity and under controllable conditions with respect to surface dimensions and densities,^[1–6] promise highly interesting physicochemical characteristics. Such properties can render these structures suitable candidates for sophisticated further applications, which comprise, e.g., the fields of biosensing,^[7–9] information storage,^[10,11] or

X. Wang, Dr. M. Sperling, Dr. M. Reifarth, Prof. A. Böker
Fraunhofer Institute for Applied Polymer Research IAP
D-14476 Potsdam-Golm, Germany
E-mail: alexander.boeker@iap.fraunhofer.de

X. Wang, Prof. A. Böker
Chair of Polymer Materials and Polymer Technologies
University of Potsdam
D-14476 Potsdam-Golm, Germany

 The ORCID identification number(s) for the author(s) of this article can be found under <https://doi.org/10.1002/sml.201906721>.

© 2020 The Authors. Published by WILEY-VCH Verlag GmbH & Co. KGaA, Weinheim. This is an open access article under the terms of the Creative Commons Attribution License, which permits use, distribution and reproduction in any medium, provided the original work is properly cited.

DOI: 10.1002/sml.201906721

be of potential use for the efficient fabrication of functional nanodevices.

2. Results and Discussion

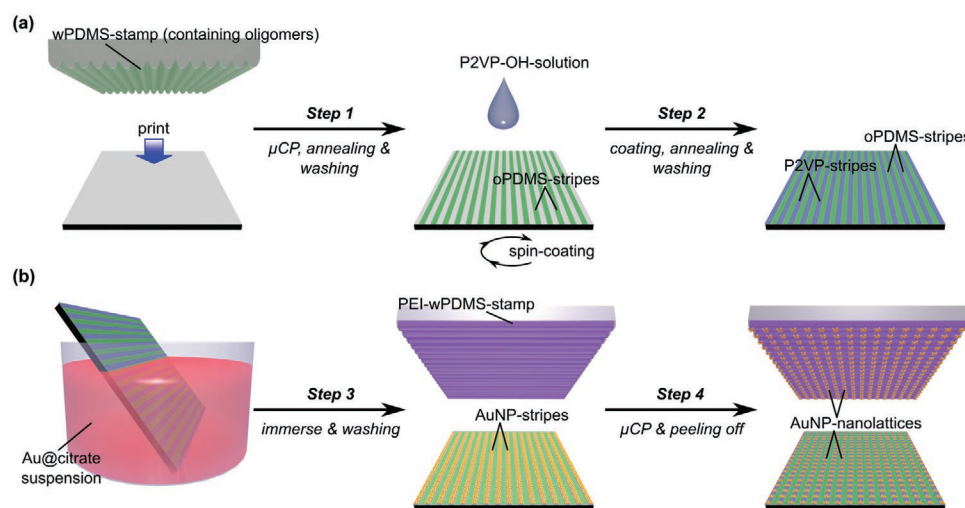
Our method to create (sub)micro-scale lattices of gold nanoparticles implements multiple μ CP as well as spin coating and solution immersion steps. A typical workflow of the procedure is depicted in **Scheme 1**. The overall process comprises two major consecutive parts, which are a routine for the preparation of a coating mask onto the surface Scheme 1a, and a routine involving the deposition and customization of nanoparticles onto said coating mask Scheme 1b. In a first step of the first routine, oligomeric polydimethylsiloxane (oPDMS) is transferred to a substrate surface from a wrinkled PDMS (wPDMS) stamp at the area of contact using μ CP, whereby silicon wafers may serve as a typical substrate. After washing and annealing, this results in the formation of a striped pattern of oPDMS, which provides a hydrophobic mask for the selective deposition with another chargeable or charged polymer on the remaining free sites via spin coating, washing, and annealing. As a result, the originally imprinted surface consists of a striped mask of alternating hydrophobic and hydrophilic stripes with a significantly differing electrostatic surface potential. In a typical routine, aiming for the deposition of negatively charged nanoparticles, the functional polymer should provide protonatable or quaternized functional groups, e.g., amino functionalities. These functional groups serve as electrostatic anchors for the deposition of oppositely charged nanoparticles from suspension as conducted in the deposition routine exemplified in Scheme 1b. Following this step, another wPDMS stamp coated with a polymer exhibiting

attractive electrostatic interaction to the as-deposited nanoparticles is brought into contact with the nanoparticulate stripe pattern, thereby selectively peeling off nanoparticles. The pattern remaining on the substrate depends on the used wPDMS dimensions (amplitude A , wavelength λ) as well as the orientation of the second wPDMS stamp during the peeling process.

In the following sections, we give a profound description of each preparation step in our routine focusing on the mechanistic details and the resulting features of the observed structures. Furthermore, we present significant results illustrating the versatility of this method.

2.1. Pre patterning with Oligomeric Polydimethylsiloxane (oPDMS, Step 1)

Wrinkled PDMS plays a central role as stamp material for the transfer of oPDMS patterns using μ CP. These stamps are feasibly prepared and easily customizable in a controlled way with respect to their microstructure.^[27] For their preparation, elastomeric PDMS substrates are converted into a mechanically stretched state (Figure S1a, Supporting Information), and subjected to a plasma treatment, which is followed by its controlled relaxation. During this tension release, the thin and rigid oxidized SiO₂-surface layer, obtained by the plasma treatment, is unable to contract—well in contrast to the elastomeric PDMS beneath said silica layer—thereby forcing the formation of surface wrinkles according to a sinusoidal shape (Figure S1b, Supporting Information). The plasma treatment conditions therefore, as also exemplified in Figure S2 in the Supporting Information, offer a precise tool for tuning the resulting wrinkle dimensions, which according to previous investigations can be



Scheme 1. General illustration of fabricating gold-nanoparticle lattices by using μ CP and wPDMS-stamps. a) Stripe pattern formation yielding a particle deposition template: Step 1 consists of a μ CP step transferring oPDMS from the top of the wrinkles to the substrate followed by annealing and washing, which results in the formation of pre-patterned hydrophobic stripes. Step 2 adds stable P2VP-OH polymer into the interspaces via spin coating from an aqueous solution, annealing and washing, which, at low pH values, results in a protonation of the surface to guide the deposition of negatively charged gold particles. b) Particle deposition and lattice customization by immersion and further μ CP: Step 3 leads to the deposition of citrate@AuNPs onto the P2VP stripes due to electrostatic interaction by immersion of the stripe pattern into an aqueous suspension of citrate-capped citrate@AuNPs with subsequent washing. In Step 4, further μ CP with a PEI-coated wPDMS-stamp (PEI-wPDMS-stamp) causes removal of citrate@AuNPs from the substrate at the area of contact leaving behind the final citrate@AuNP-nanolattices.

attributed to the change in thickness and mechanical modulus of said rigid silica surface layer.^[34,41,43–46] As a substrate, silicon wafers provide a material with a very pronounced smoothness along with a defined chemical composition of the surface. This, accordingly, renders them very suitable for the creation of surface patterns and their subsequent characterization.

We achieve an initial surface patterning by placing a freshly prepared wPDMS stamp on the Si wafer substrate. Noteworthy, Step 1 of Scheme 1 represents a rather unconventional μ CP variation, as no additional ink is required. Instead, this process relies on the transfer of oPDMS from the wPDMS stamp to the substrate. The oPDMS originates from precursor materials that remain unreacted during the curing process of the PDMS elastomer and is, thus, intrinsically present within the matrix of the stamp. Accordingly, these stamps can be considered as self-inking, which is quite convenient, since it simplifies the μ CP routine. Furthermore, ink transfer merely occurs at the contacted area, and oPDMS will only functionalize the bare substrate at the wrinkle tips of the wPDMS stamps during the printing process. As a result, stable hydrophobic oPDMS stripes form on the substrate.

We implemented atomic force microscopy to investigate the morphology of the oPDMS-functionalized substrates. A corresponding AFM image of the substrate wafer immediately after the μ CP process is shown in Figure 1a (height image and corresponding height profile). Indeed, we can observe the presence of a striped pattern on the substrate showing a maximum height of about ≈ 30 nm, while experiencing a significant decrease to ≈ 10 – 15 nm, after washing and annealing. In contrast thereto, the wavelength remains constant at $1.7 \mu\text{m}$. This observation can be explained by the fact that unbound oPDMS material is removed during this washing step, so that only covalently bound, and hence, immobilized material remains on the wafer surface. Moreover, the morphology seems to change toward a triple peak

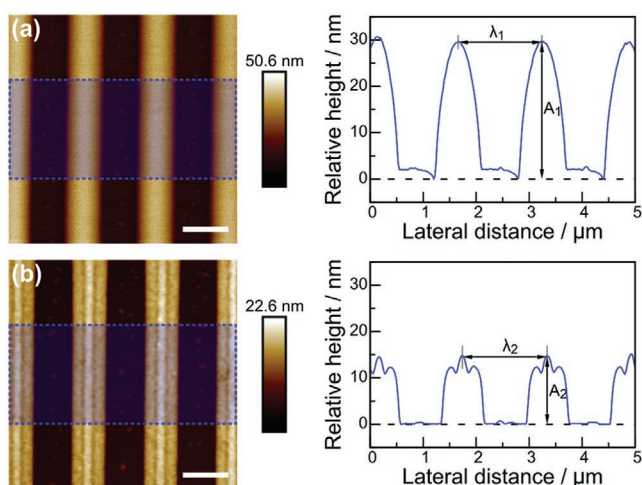


Figure 1. AFM-height images of oPDMS stripes with corresponding height profiles: a) before and b) after annealing and washing treatments. In the right column, the respective height profiles corresponding to the area highlighted by the dashed blue boxes are shown. For visualization, the wavelengths (λ) and amplitudes (A) of the stripes are indicated by the black arrows: (a) $\lambda_1 = 1.7 \mu\text{m}$, $A_1 = 30$ nm; (b) $\lambda_2 = 1.7 \mu\text{m}$, $A_2 = 15$ nm. As it can be seen, the annealing process leads to a substantial decrease in stripe amplitude (by about 50%), while the wavelength stays constant (Scale bars: $1 \mu\text{m}$).

shape, whereby the overall feature width remains constant. A possible explanation for this observation could be a collapsing oPDMS framework during annealing caused by removal of traces of solvent, yielding a wrinkled peak morphology.

Here, one might argue that the stripe morphology originates from a transfer of pieces of PDMS, which are torn out from the stamp upon its removal during the μ CP process rather than being a result of oPDMS transfer. However, in that case an inhomogeneous stripe morphology due to uncontrollable tearing out of PDMS would be expected. Accordingly, also the wPDMS stamps should show an inhomogeneous surface corresponding to the stripe morphology. In our experiments, however, we were not able to observe such an effect. On the contrary, we observe smooth profiles along the wrinkle surface as well as the oPDMS stripes before and after the μ CP process, as illustrated in Figures S3 and S4 in the Supporting Information. Furthermore, also a high degree of reproducibility of the thicknesses of the imprinted stripes hints toward the rather controlled process of oPDMS transfer (Figure S5, Supporting Information). We, for the sake of completeness, additionally mention here that we were not able to achieve regular oPDMS patterns at wavelengths $< 0.7 \mu\text{m}$ due to the merge of the resulting stripes by smearing effects (Figure S6, Supporting Information).

Concerning the chemistry of oPDMS, the oPDMS species originate from PDMS precursor materials, namely methylvinylsiloxane-dimethylsiloxane copolymers forming the polymeric backbone and methylhydrosiloxane-dimethylsiloxane as cross-linker, which remain unbound and floating within the PDMS network. These oligomers can react actively with the silanol groups on the oxidized surface of the activated Si-wafer yielding covalent $-\text{Si}-\text{O}-\text{Si}-$ bonds, whereby a precedent hydrolysis step triggers the condensation reaction.^[47] Said hydrolysis process is moisture-dependent since the presence of water promotes the formation of silanol groups. Accordingly, higher humidity during the printing process could enhance the success of stripe formation. The detailed experimental investigation process with respect to humidity conditions is discussed in the supporting information (Figure S7, Supporting Information). In order to gain an even more profound understanding of the printing process, we aimed for the elucidation of the chemical characteristics of the printed oligomer patterns.^[48–50] For this purpose, angle resolved X-ray photoelectron spectroscopy (AR-XPS, Figure S8, Supporting Information) was employed. At a take-off angle of 20° , these measurements revealed an approximate elemental molar ratio $[\text{O}]/[\text{Si}]$ of ≈ 1 within the siloxane network, which is expected for PDMS.^[48,51–53] We would like to note here, that at a take off angle of 20° , the analysis depth of the X-ray beam reduces to 3.4 nm (compared to 10 nm at 90°). Therefore, the XPS signal of the oPDMS stripes (≥ 15 nm height) can be isolated from the underlying substrate surface. Consequently, these observations further solidify the concept of oPDMS transfer. For more details about the AR-XPS measurements, we would like to refer the interested reader to the Supporting Information of this article (Figure S9 and Table S1, Supporting Information).

2.2. Backfilling of oPDMS Stripes with P2VP-OH (Step 2)

Its natural occurrence within commonly prepared PDMS represents a rather useful aspect of oPDMS, which could be exploited

to create a structured hydrophobic pattern on a silicon wafer in a straightforward fashion. Moreover, we were interested, to which extent these patterns can promote further surface functionalization. Accordingly, we modified the oPDMS-stripped pattern by spin coating an aqueous solution of poly(2-vinylpyridine-co-2-hydroxyethyl acrylate), which we will further on refer to as P2VP-OH for the polymer in solution and as P2VP for the surface bound molecules, respectively (Step 2 of Scheme 1). The experimental preparation as well as the characterization details of the P2VP-OH are presented in the Supporting Information (Figure S10 and Table S2, Supporting Information). Owing to the hydrophobic nature of the oPDMS stripes, the hydrophilic P2VP-OH is expected to accumulate exclusively within the interspaces and, thus, to backfill the gaps in-between said stripes forming a striped pattern of alternating oPDMS and P2VP. In analogy to oPDMS, the P2VP-OH, undergoes an annealing process after coating, during which the hydroxyl groups in the side chains of the polymeric framework of P2VP-OH are expected to form silica esters with the Si-OH groups on the free activated wafer surface.^[54,55] Accordingly, this would result in the covalent attachment of the polymer to the substrate surface and, therefore enhance its adhesion thereon. In order to examine the chemical nature of oPDMS–P2VP substrate in more detail, XPS measurements were performed on a substrate as shown in the Supporting Information of the article (Figure S11, Supporting Information). The presence of the characteristic XPS signal for nitrogen on the washed substrate strongly suggests the successful deposition of the P2VP-OH. For further elucidation of the morphology of the oPDMS–P2VP patterns, different AFM techniques were employed and summarized in **Figure 2**. We provide the AFM results of the oPDMS patterns (Figure 2a) alongside the respective characteristics of the oPDMS–P2VP templates (Figure 2b) for comparison. In a

first instance, height profiles were acquired which are displayed as a blue line plot in Figure 2. A thorough comparison of both height profiles, thereby, reveals an insignificant height difference between the different stripe domains in both plots (merely 1–2 nm). Hence, this method alone cannot sufficiently answer the question whether the P2VP-OH polymer exclusively backfills the gaps between the oPDMS stripes. For deeper investigations, further AFM modes were performed, such as phase contrast imaging, which depends on many material properties such as adhesion, stiffness, and friction (see tapping mode AFM results in Figure S12 in the Supporting Information).^[56,57] The frequency-modulated Kelvin probe force microscopy (FM-KPFM), however, promises to provide a more pronounced contrast here. KPFM is very sensitive to even small differences in work functions of materials, which in turn depend on surface potential. This renders this technique a suitable method to unravel the lateral inhomogeneities in surface potential.^[58–61] The difference in surface potential is given by the contact potential difference (CPD) value ΔCPD (Equation (1))

$$\Delta\text{CPD} = \frac{|\Phi_{\text{tip}} - \Phi_{\text{sample}}|}{e} \quad (1)$$

where Φ_{tip} and Φ_{sample} are the work functions of the tip and sample, respectively, and e represents the elementary charge.^[61] Considering a structured substrate pattern consisting of two distinct domains, ΔCPD simply translates to Equation (2)

$$\Delta\text{CPD}_{\text{domains}} = 1/e |\Phi_{\text{tip}} - \Phi_{\text{domain},1} - (\Phi_{\text{tip}} - \Phi_{\text{domain},2})| = 1/e |\Phi_{\text{domain},1} - \Phi_{\text{domain},2}| \quad (2)$$

where domain 1 represents the oPDMS-stripped area and domain 2 represents the interspaces.

The potential curves resulting from KPFM measurements are drawn in red within the plots of Figure 2. A thorough investigation reveals that ΔCPD on the surface of the oPDMS-stripped wafer is significantly less pronounced than for the oPDMS–P2VP wafers (180 mV vs 470 mV). According to previous literature, it can be expected that the potential difference stays lower between SiO₂/oPDMS in comparison to P2VP/oPDMS.^[62–64] The samples presented in Figure 2 indeed follow this trend, which essentially underlines our hypothesis that P2VP-OH selectively covers the SiO₂ domains of the sample within the interspaces of the oPDMS stripes.

At this point, we would like to remind the reader of the tunability of the oPDMS stripes' wavelength (Figures S2 and S5, Supporting Information). This tunability readily translates into the adjustability of the oPDMS–P2VP patterns, and therefore enables a high degree of customization of the stripe dimensions. This so formed mask serves as an efficient guide for the deposition of charged particles from suspension as will be further described in the following section.

2.3. Deposition of Citrate Stabilized Gold Nanoparticles (Step 3)

The preparation steps discussed above allow for the creation of mask onto a flat surface, which exhibits alternating oPDMS and P2VP stripes. In a moist atmosphere, the pyridine containing moieties of the P2VP domains partially show a positive charge

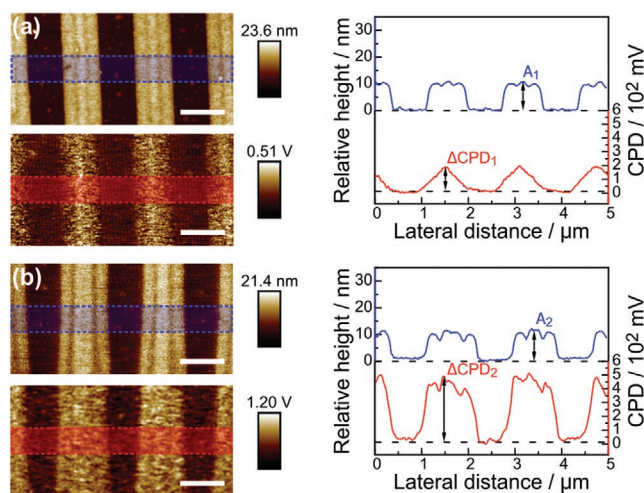


Figure 2. The FM-KPFM potential images: a) pristine oPDMS samples and b) oPDMS–P2VP. The left column shows the height (top) and potential profiles (bottom). In the right column, the corresponding profile graphs are given, with the height profile shown in blue and the potential given in red. Even though the height differences between (a) and (b) do not vary notably, the potential curves show that this difference rises after coating with P2VP-OH, thereby proving its collection in-between the oPDMS domains. The scale bars are 1 μm .

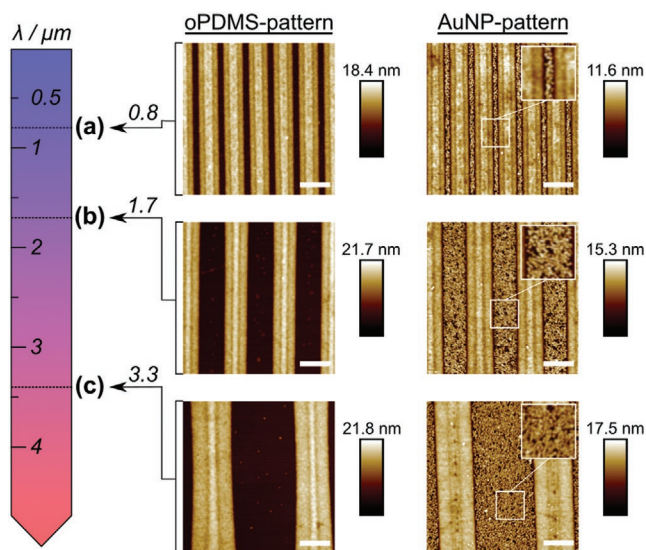


Figure 3. Citrate@AuNP stripe patterns (right column images) for oPDMS patterns (left column images) with differently prepared wavelengths λ by using the appropriately sized wPDMS-stamps during the μ CP process (Step 1, Scheme 1). The dimensions of the citrate@AuNP stripes directly depend on the stripe pattern provided by oPDMS transferred by the wPDMS-stamp: a) 0.8 μm , b) 1.7 μm , c) 3.3 μm . The insets within the citrate@AuNP pattern images show the indicated zoom-in areas containing the particles. The scale bars are 1 μm .

due to protonation, which is well in contrast to the neutral oPDMS. Consequently, the prepared oPDMS–P2VP patterns may serve as a guiding template for the assembly of negatively charged nanoparticles, which can adhere to the P2VP domains due to their electrostatic interaction. For this purpose, citrate stabilized gold nanoparticles (citrate@AuNPs) were employed (≈ 15 nm, Figure S13, Supporting Information). The particle suspension used throughout our experiments possessed a pH value of ≈ 5.5 . This pH approximately matches that of the pyridine moieties of the P2VP domains leaving a substantial amount thereof in a protonated state.^[65–67] Thus, by immersing the oPDMS–P2VP patterned substrates in the citrate@AuNP suspension (Step 3 of Scheme 1), the particles get electrostatically adsorbed onto the P2VP domains. **Figure 3** shows exemplary AFM images of the initial oPDMS striped samples (left column) and the correspondingly resulting citrate@AuNP stripes (right column) for differently prepared wavelengths λ . These images clearly depict the presence of striped domains of closely packed citrate@AuNPs. The adjustability of the stripe dimensions directly converts into a high variety of the nanoparticle stripes, as illustrated in Figure 3. Here, we show representative examples of differently dimensioned citrate@AuNP stripes with the wavelengths of a) 0.8 μm , b) 1.7 μm , and c) 3.3 μm , respectively.

2.4. Particle Removal with a Further Wrinkled Stamp (Step 4)

Striving for even more complexity of the created lattice structures, we applied a peeling off-step to the as-formed citrate@AuNP stripes by employing a second μ CP-step with another

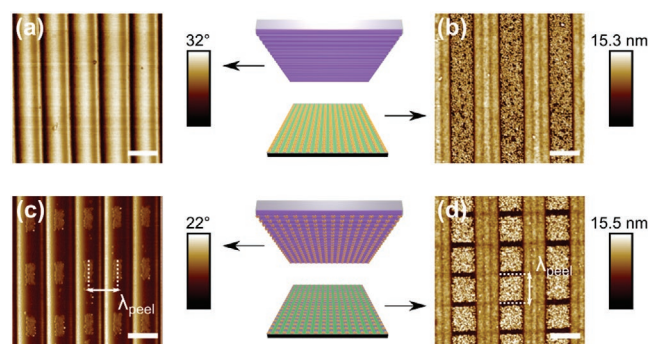


Figure 4. Investigation of the peeling-off process to create the citrate@AuNP nanolattices: a) PEI-wPDMS-stamp and b) citrate@AuNP stripes before peeling-off; c) PEI-wPDMS-stamp and d) citrate@AuNP quadrangular nanolattices after peeling-off. AFM data is shown as phase images for the stamps and height images for the citrate@AuNP-structured samples, respectively. citrate@AuNPs are withdrawn exclusively from the substrate at the area of contact with the PEI-wPDMS-stamp ($\lambda_{\text{peel}} \approx 0.95$ μm) as it can be seen by the fact that the particle fields deposited on the PEI-wPDMS stamp (c) correspond to the gaps at the substrate (d). The scale bars are 1 μm .

wPDMS stamp (Step 4, Scheme 1). This second μ CP step leads for instance to the preparation of rectangularly shaped patterns as depicted in **Figure 4**. Therefore, the second stamp needs to be tailored in such a way that it attracts the particles to a greater extent than compared to the P2VP-decorated substrate. This was achieved by employing a PEI-wPDMS (polyethylenimine-coated wPDMS) stamp (Figure 4a), whereby PEI was utilized as branched derivative. The PEI-wPDMS stamp is placed on the citrate@AuNP-stripe surface, which is again depicted in Figure 4b. The orientation of the grooves of this PEI-wPDMS stamp in this case was in an orthogonal direction to the orientation of the citrate@AuNP stripes, whereupon citrate@AuNPs at the area of contact transfer from the substrate wafer to the PEI-wPDMS stamp. Figure 4c shows the transferred citrate@AuNPs rectangles on the PEI-wPDMS stamp after the peeling step. The dimensions of the rectangles are $\approx 0.18 \times 0.8$ μm . The citrate@AuNPs remaining on the wafer substrate form lattice squares with dimensions of $\approx 0.8 \times 0.8$ μm as exemplified in Figure 4d. There, the gaps of $\approx 0.18 \times 0.8$ μm between the squares along the original citrate@AuNP stripe direction correspond to the rectangularly shaped particle fields at the PEI-wPDMS stamp. It can, therefore, be concluded here, that the dimensions of the wPDMS stamp (λ_{wPDMS} , step 1, Scheme 1) and the one used for the peeling step (λ_{peel} , step 4, Scheme 1) determine the dimensions of the formed citrate@AuNP rectangular lattices.

In the aforementioned case, printing with a wPDMS-stamp with $\lambda_{\text{wPDMS}} \approx 1.7$ μm and peeling with a PEI-wPDMS with $\lambda_{\text{peel}} \approx 0.95$ μm led to square citrate@AuNP lattices with an area of about ≈ 0.8 $\mu\text{m} \times 0.8$ μm . We were curious, to which extent variations in the peeling-off process of the particles would allow to produce more shape variety of the resulting citrate@AuNP lattices. Accordingly, we varied the i) dimensions of the citrate@AuNP stripes, ii) wavelengths of the utilized PEI-wPDMS stamps, and iii) lateral rotation angle α between the citrate@AuNP stripe direction and the orientation PEI-wPDMS stamps. The results are demonstrated with SEM images in **Figure 5**.

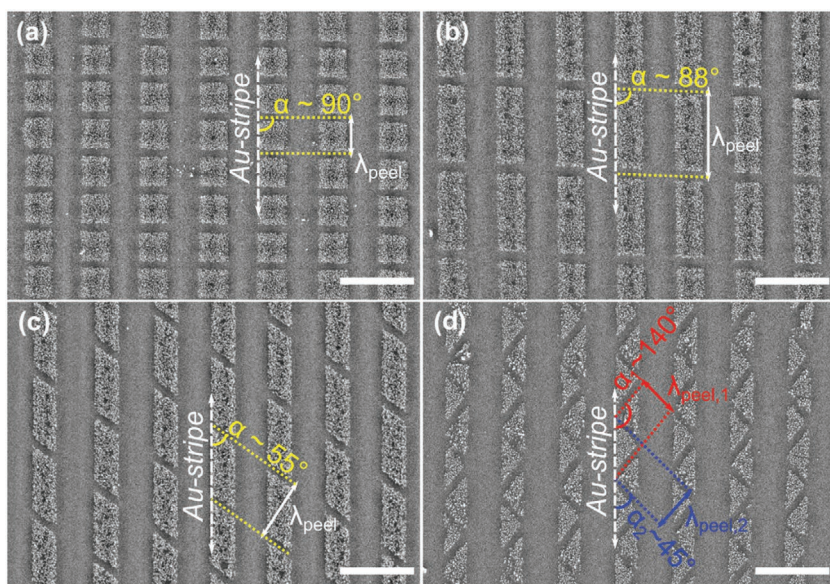


Figure 5. SEM images of different citrate@AuNP nanolattices prepared by tuning the wavelength λ_{peel} of the PEI-wPDMS stamps used for the peeling step(s); the wavelength of the first wPDMS was kept constant at $\lambda_{\text{wPDMS}} \approx 1.7 \mu\text{m}$: a) square units ($\lambda_{\text{wPDMS}} > \lambda_{\text{peel}} \approx 0.95 \mu\text{m}$); b) rectangular units ($\lambda_{\text{wPDMS}} < \lambda_{\text{peel}} \approx 2.50 \mu\text{m}$); c) parallelogram unit ($\lambda_{\text{wPDMS}} < \lambda_{\text{peel}} \approx 2.3 \mu\text{m}$) at a rotation angle $\alpha \approx 55^\circ$; d) two peeling-off step ($\lambda_{\text{peel},1} = \lambda_{\text{peel},2} \approx 1.10 \mu\text{m}$) with $\alpha_1 \approx 140^\circ$ and $\alpha_2 \approx 45^\circ$; α represents the lateral rotation angle of the PEI-wPDMS-stamp with respect to the citrate@AuNP-stripes. Depending on the dimensions of the stamps and orientation angle α , a high degree of pattern customization is accessible. The scale bars are $2 \mu\text{m}$.

The dimension tunability of citrate@AuNP stripes was exemplified in Figure 3. We altered the wavelength of the PEI-wPDMS stamp for the peeling step (λ_{peel}) at a constant $\lambda_{\text{wPDMS}} \approx 1.7 \mu\text{m}$. When the rotation angle α was 90° , a λ_{peel} of $\approx 0.95 \mu\text{m}$ led to the formation of quadratic (Figure 5a), while $\approx 2.50 \mu\text{m}$ yielded rectangular citrate@AuNP lattices (Figure 5b), respectively. Variation of the rotation angle α of the PEI-wPDMS stamp with respect to the citrate@AuNP stripes led to different lattice structures. Figure 5c, for instance, shows parallelogram lattices for $\alpha \approx 55^\circ$. We implemented even more complex citrate@AuNP lattices by using a second peeling-off step. Here, we were able to create triangular patterns as shown in Figure 5d. Note, that the fabrication of triangularly shaped nanolattices requires a careful adjustment of all dimensions of the citrate@AuNP stripes and stamps as well as rotation angles α_i (α_i indicating rotation angles of the peeling-off steps). If carefully adjusted, these parameters serve as a powerful tool for the creation of highly complex periodic surface patterns made from nanoparticulate materials.

3. Conclusion

We were able to develop a straightforward, scalable and cost-efficient method for the fabrication of sophisticated and highly customizable nanolattice patterns by a dedicated series of micro-contact printing and surface coating steps. The process relies on wrinkled PDMS stamps that can be precisely tuned in terms of groove dimensions, e.g., wavelength, via appropriate preparation conditions. These stamps natively contain free oligomeric

PDMS, which can be transferred readily to a substrate surface via a simple microcontact printing routine. This led to the formation of a stable periodic stripe pattern on the substrate after annealing and washing, whereby its dimensions directly correspond to that of the wrinkles. Accordingly, a heterogeneous surface chemistry is created allowing for the entrapment of polymers, such as P2VP-OH, in-between the oligomer stripes. When using polymers able to exhibit electrostatic charge, e.g., upon protonation, these polymer stripes can serve as basis for the deposition of oppositely charged nanoparticles from suspension yielding defined nanoparticle stripes, which we demonstrated by using negatively charged citrate@AuNPs for the positive P2VP stripes. Further shaping into complex geometries, such as quadrangular or triangular, can be achieved by selectively peeling-off citrate@AuNPs using another wrinkled PDMS stamp, which possesses an increased affinity of the nanoparticles compared to the substrate. Due to the high tunability of the wrinkle dimensions along with the adjustability of the lateral rotation of the stamp toward the formed nanoparticle stripes during the peeling-off step, our method offers an extraordinarily high degree of freedom in terms of aspect ratio and angu-

larity of the resulting shapes. Furthermore, this method can be applied to various kinds of flat silicon-based surfaces. We therefore believe that this new workflow, being easy to realize even on a larger scale and avoiding the need of expensive lithographic techniques for surface patterning, may serve as a powerful tool for the creation of highly sophisticated nanoparticle surface patterns of various materials, shapes, and functionality.

4. Experimental Section

Materials and Devices: PDMS was obtained as a Sylgard 184 elastomer kit, consisting of prepolymer and crosslinker at a ratio of 10:1, from Dow Corning Company. Silicon Wafers (1,0,0), p-Type, CrysTech) with thin oxidized layer were cleaned with ethanol first, then treated with SC1 solution (Standard Clean), which consists of NH_4OH (28–30 wt% NH_3 basis, ACS reagent, Sigma), H_2O_2 (30% wt%, reag. Ph. Eur., Sigma) and Milli-Q H_2O (18.2 M Ω cm at 25 °C, Milli-Q Reference from Merck) at a ratio of 1:1:5.^[68] In brief, the wafers were immersed into SC1 solution at 70 °C for 10 min, then washed with Milli-Q water thoroughly and dried in air. The hydroxyl-functional polymer poly(2-vinyl pyridine-co-2-hydroxyethyl acrylate) (referred to as P2VP-OH), was synthesized by radical copolymerization method, and the detailed preparation and characterization are shown in the Supporting Information (Figure S10 and Table S2, Supporting Information). Gold(III) chloride trihydrate ($\geq 99\%$, Sigma), sodium citrate hydrate ($\geq 99\%$, Sigma), branched polyethylenimine ($M_w = 25\,000 \text{ g mol}^{-1}$, $\leq 1\%$ water, Sigma) and other solvents in this paper were used as purchased. The spin coater instrument was obtained from Laurell Technologies Corporation, Spin Coater WS-650MZ-23NPPB. The plasma oven was obtained from Plasma Technology, PlasmaFlecto 10.

Atomic Force Microscopy (AFM): Tapping mode AFM images were recorded on a Bruker Dimension Icon using with OTESPA-R3 tips

($k = 26 \text{ N m}^{-1}$, $f_0 = 300 \text{ kHz}$). Kelvin probe force microscopy (KPFM) images were obtained by FM-KPFM mode, and the tip used was SCM-PIT-V2 with $k = 3.0 \text{ N m}^{-1}$, $f_0 = 75 \text{ kHz}$. In the FM-KPFM, the contact potential difference (CPD) between the dip and sample surface was measured, and the potential image was obtained to show the CPD changing along with lateral dimension. The measuring software for tapping mode and FM-KPFM mode was Nanoscope 9.1, and all the images were processed by using Nanoscope Analysis 1.5.

Scanning Electron Microscope (SEM): The SEM images were acquired with a GeminiSEM 300 scanning electron microscope (Zeiss) with an acceleration voltage of 5 kV. The samples were adhered to a conductive bottom surface. Afterward, the samples were sputtered with a platinum layer (thickness 4 nm) to avoid electrical charging.

Fabrication of Oligomeric PDMS (oPDMS) Stripes on Oxidized Silicon Wafers: First, the flat PDMS substrates with the thickness of 2 mm were prepared by mixing and curing prepolymer and cross-linker at a weight ratio of 10:1. For this purpose, 32 g mixture was blended thoroughly, and poured into a clean and plane Petri dish (12 cm × 12 cm × 12 mm). After the removal of air bubbles by leaving the mixture at room temperature for 24 h, the substrates were cured at 80 °C for 2 h. These substrates were cut into stripes with the dimension of 25 mm × 10 mm × 2 mm to be used.

Second, the stripes were stretched to 130% of their original length by using a custom-made stretching apparatus (Figure S1a, Supporting Information). Remaining in this stretched state, the aforesaid stripes were exposed to O₂ plasma (0.1 mbar, 100 W) for 30 s and released gradually to form wrinkled stamps, referred to as wPDMS stamps. The wPDMS stamps with different wavelengths were prepared by differing the treating time and treating pressure in this paper, and the detailed process is shown in the experimental area of Figure S2 in the Supporting Information. Note, that even though the wrinkle dimensions on a single stamp showed a rather low standard deviation, the wavelength dimensions of numerous wrinkle stamps prepared under reproduced experimental conditions could deviate up to 10% due to the changes of humidity and temperature inside the plasma chamber.^[69]

For μ CP, the prepared stamps were diced into 10 mm × 10 mm pieces and printed on the cleaned silicon wafers (10 mm × 10 mm). The stamps were left on the wafers for 12 h without additional pressure, and then peeled off from the wafers. The wafers were put into a drying oven to carry on the annealing treatment under vacuum (5 mbar) at 130 °C for 5 h. The annealed samples were washed with toluene, acetone and Milli-Q water sequentially and thoroughly to get stable stripe patterns, referred to as oPDMS stripes. These stripes were characterized by AFM and XPS measurements.

Preparation of (Oligomer PDMS)-Poly(2-Vinyl Pyridine) Stripe Patterns (oPDMS-P2VP): The P2VP-OH solution in chloroform (1%, w/v) was spin coated on oPDMS stripes (30 s, 2000 rpm, and 2000 acceleration), and the samples were annealed in vacuum oven (5 mbar) for 3 h at 110 °C. Afterward, these samples were washed with tetrahydrofuran thoroughly to obtain the stable oPDMS-P2VP patterns. AFM and XPS were used for the characterizations.

Creation of Metallic Nanolattices on oPDMS-P2VP Patterns: The prepared oPDMS-P2VP patterns were immersed in a suspension of citrate-stabilized gold nanoparticles (citrate@AuNPs) for 10 min, and the obtained samples were washed with Milli-Q water thoroughly to obtain citrate@AuNP stripes. The suspension of citrate@AuNPs was obtained by Frens method and used as prepared in the course of this study.^[70] Typically, 2 mL $34 \times 10^{-3} \text{ M}$ trisodium citrate aqueous solution was added into 50 mL $0.5 \times 10^{-3} \text{ M}$ HAuCl₄ solution (sub-boiling at 94 °C) quickly with strong stirring. After 10 min, the mixture turned into fresh red, indicating citrate@AuNPs formed. TEM, DLS, and UV-vis spectroscopy were implemented to characterize the obtained AuNP@citrate (Figure S13, Supporting Information).

To form citrate@AuNP lattices, a PEI-wPDMS stamp (10 mm × 10 mm) was placed on the citrate@AuNP stripes, in which the groove direction of the stamp was placed with perpendicular orientation to citrate@AuNP stripes. A 30 g weight was placed on the PEI-wPDMS stamp to ensure the conformal contacting. After 12 h, the PEI-wPDMS

stamp was removed to peel off parts of citrate@AuNP s from the citrate@AuNP stripes, which had been in contact to the wrinkle tips, so that nanoparticle lattices could be prepared. The printing process was repeated with differently dimensioned PEI-wPDMS stamps as well as lateral rotation angle between the groove orientation of the stamps and the citrate@AuNP-stripe direction. Consequently, many kinds of citrate@AuNP nanolattices could be formed. For characterization, AFM and SEM were used. The PEI-wPDMS stamps were obtained by immersing the plasma-activated wrinkled stamp (0.2 mbar, 100 W, 1 min, O₂ plasma) into a 5% (w/v) PEI aqueous solution for 30 min. Afterward, they were washed with Milli-Q water and then dried with air thoroughly.

Supporting Information

Supporting Information is available from the Wiley Online Library or from the author.

Acknowledgements

This research has received funding from Volkswagen Foundation (FR: 91791) and European Research Council (Replicoll: 648365). The authors thank Dr. Nikolay Puresky for introducing X.W. to several characterization techniques and for giving some useful advices. The authors sincerely thank Dr. Andreas Holländer for his support for XPS measurements, and Steffi Grunst's support in preparing SEM images. X.W. thanks the China Scholarship Council for the personal financial support.

Conflict of Interest

The authors declare no conflict of interest.

Keywords

gold nanoparticle assembly, hydroxyl-functional poly(2-vinyl pyridine), metallic nanolattices, microcontact printing, oligomeric polydimethylsiloxane, polydimethylsiloxane wrinkles, wrinkled stamps

Received: November 19, 2019

Revised: January 24, 2020

Published online: February 24, 2020

- [1] L. Jiang, X. Chen, N. Lu, L. Chi, *Acc. Chem. Res.* **2014**, *47*, 3009.
- [2] K. D. Alexander, M. J. Hampton, S. Zhang, A. Dhawan, H. Xu, R. Lopez, *J. Raman Spectrosc.* **2009**, *40*, 2171.
- [3] M. S. Onses, C. C. Liu, C. J. Thode, P. F. Nealey, *Langmuir* **2012**, *28*, 7299.
- [4] D. Nepal, M. S. Onses, K. Park, M. Jespersen, C. J. Thode, P. F. Nealey, R. A. Vaia, *ACS Nano* **2012**, *6*, 5693.
- [5] S. Gwo, M. H. Lin, C. L. He, H. Y. Chen, T. Teranishi, *Langmuir* **2012**, *28*, 8902.
- [6] H. Zhang, J. Cadusch, C. Kinnear, T. James, A. Roberts, P. Mulvaney, *ACS Nano* **2018**, *12*, 7529.
- [7] F. Sun, H. C. Hung, A. Sinclair, P. Zhang, T. Bai, D. D. Galvan, P. Jain, B. Li, S. Jiang, Q. Yu, *Nat. Commun.* **2016**, *7*, 13437.
- [8] J. Baumberg, S. Bell, A. Bonifacio, R. Chikkaraddy, M. Chisanga, S. Corsetti, I. Delfino, O. Eremina, C. Fasolato, K. Faulds, H. Fleming, R. Goodacre, D. Graham, M. Hardy, L. Jamieson,

- T. Keyes, A. Królikowska, C. Kuttner, J. Langer, C. Lightner, S. Mahajan, J.-F. Masson, H. Muhamadali, M. Natan, F. Nicolson, E. Nikelsch, K. Plakas, J. Popp, M. Porter, D. Prezgot, N. Pytlík, S. Schlücker, A. Silvestri, N. Stone, Z. Q. Tian, A. Tripathi, M. Willner, P. Wuytens, *Faraday Discuss.* **2017**, 205, 429.
- [9] J. N. Anker, W. P. Hall, O. Lyandres, N. C. Shah, J. Zhao, R. P. Van Duyne, *Nat. Mater.* **2008**, 7, 442.
- [10] H. Ditlbacher, J. R. Krenn, B. Lamprecht, A. Leitner, F. R. Aussenegg, *Opt. Lett.* **2000**, 25, 563.
- [11] J. Lee, B. Yoo, H. Lee, G. D. Cha, H. S. Lee, Y. Cho, S. Y. Kim, H. Seo, W. Lee, D. Son, M. Kang, H. M. Kim, Y. I. Park, T. Hyeon, D. H. Kim, *Adv. Mater.* **2017**, 29, 1603169.
- [12] C. Matricardi, C. Hanske, J. L. Garcia-Pomar, J. Langer, A. Mihi, L. M. Liz-Marzán, *ACS Nano* **2018**, 12, 8531.
- [13] K. Vogele, J. List, G. Pardatscher, N. B. Holland, F. C. Simmel, T. Pirzer, *ACS Nano* **2016**, 10, 11377.
- [14] H. A. Atwater, A. Polman, *Nat. Mater.* **2010**, 9, 205.
- [15] Y. Yao, L. Zhang, T. Leydecker, P. Samori, *J. Am. Chem. Soc.* **2018**, 140, 6984.
- [16] K. Sumaru, T. Takagi, K. Morishita, T. Satoh, T. Kanamori, *Soft Matter* **2018**, 14, 5710.
- [17] R. Maoz, J. Berson, D. Burshtain, P. Nelson, A. Zinger, O. Bitton, J. Sagiv, *ACS Nano* **2018**, 12, 9680.
- [18] P. Schnauber, J. Schall, S. Bounouar, T. Höhne, S. I. Park, G. H. Ryu, T. Heindel, S. Burger, J. D. Song, S. Rodt, S. Reitzenstein, *Nano Lett.* **2018**, 18, 2336.
- [19] R. D. Piner, J. Zhu, F. Xu, S. Hong, C. A. Mirkin, *Science* **1999**, 283, 661.
- [20] D. S. Ginger, H. Zhang, C. A. Mirkin, *Angew. Chem., Int. Ed.* **2004**, 43, 30.
- [21] H. S. Suh, D. H. Kim, P. Moni, S. Xiong, L. E. Ocola, N. J. Zaluzec, K. K. Gleason, P. F. Nealey, *Nat. Nanotechnol.* **2017**, 12, 575.
- [22] Q. Li, J. He, E. Glogowski, X. Li, J. Wang, T. Emrick, T. P. Russell, *Adv. Mater.* **2008**, 20, 1462.
- [23] Z. Liu, H. Huang, T. He, *Small* **2013**, 9, 505.
- [24] K. W. Oleske, K. P. Barteau, M. Z. Turker, P. A. Beaucage, L. A. Estroff, U. Wiesner, *Macromolecules* **2017**, 50, 542.
- [25] S. Alom Ruiz, C. S. Chen, *Soft Matter* **2007**, 3, 168.
- [26] S. S. Chae, H. Min, J. H. Lee, B. Hwang, W. M. Sung, W. S. Jang, Y. B. Yoo, J. Oh, J. H. Park, D. Kang, D. Kim, Y. S. Kim, H. K. Baik, *Adv. Mater.* **2013**, 25, 1408.
- [27] D. John, M. Zimmermann, A. Böker, *Soft Matter* **2018**, 14, 3057.
- [28] A. Kumar, G. M. Whitesides, *Appl. Phys. Lett.* **1993**, 63, 2002.
- [29] A. Kumar, H. A. Biebuyck, G. M. Whitesides, *Langmuir* **1994**, 10, 1498.
- [30] K. Efimenko, M. Rackaitis, E. Manias, A. Vaziri, L. Mahadevan, J. Genzer, *Nat. Mater.* **2005**, 4, 293.
- [31] M. Nania, F. Foglia, O. K. Matar, J. T. Cabral, *Nanoscale* **2017**, 9, 2030.
- [32] S. Yang, K. Khare, P. C. Lin, *Adv. Funct. Mater.* **2010**, 20, 2550.
- [33] C. M. Stafford, C. Harrison, K. L. Beers, A. Karim, E. J. Amis, M. R. VanLandingham, H. C. Kim, W. Volksen, R. D. Miller, E. E. Simonyi, *Nat. Mater.* **2004**, 3, 545.
- [34] S. Hiltl, M. P. Schürings, A. Balaceanu, V. Mayorga, C. Liedel, A. Pich, A. Böker, *Soft Matter* **2011**, 7, 8231.
- [35] H. Endo, Y. Mochizuki, M. Tamura, T. Kawai, *Colloids Surf. A* **2014**, 443, 576.
- [36] H. Endo, Y. Mochizuki, M. Tamura, T. Kawai, *Langmuir* **2013**, 29, 15058.
- [37] N. Pazos-Pérez, W. Ni, A. Schweikart, R. A. Alvarez-Puebla, A. Fery, L. M. Liz-Marzán, *Chem. Sci.* **2010**, 1, 174.
- [38] C. Hanske, M. Tebbe, C. Kuttner, V. Bieber, V. V. Tsukruk, M. Chanana, T. A. F. König, A. Fery, *Nano Lett.* **2014**, 14, 6863.
- [39] A. M. Steiner, M. Mayer, M. Seuss, S. Nikolov, K. D. Harris, A. Alexeev, C. Kuttner, T. A. F. König, A. Fery, *ACS Nano* **2017**, 11, 8871.
- [40] A. Horn, S. Hiltl, A. Fery, A. Böker, *Small* **2010**, 6, 2122.
- [41] M. Pretzl, A. Schweikart, C. Hanske, A. Chiche, U. Zettl, A. Horn, A. Böker, A. Fery, *Langmuir* **2008**, 24, 12748.
- [42] R. Prathapan, J. D. Berry, A. Fery, G. Garnier, R. F. Tabor, *ACS Appl. Mater. Interfaces* **2017**, 9, 15202.
- [43] M. Muller, M. Karg, A. Fortini, T. Hellweg, A. Fery, *Nanoscale* **2012**, 4, 2491.
- [44] F. A. Bayley, J. L. Liao, P. N. Stavrinou, A. Chiche, J. T. Cabral, *Soft Matter* **2014**, 10, 1155.
- [45] M. Nania, O. K. Matar, J. T. Cabral, *Soft Matter* **2015**, 11, 3067.
- [46] B. A. Glatz, A. Fery, *Soft Matter* **2019**, 15, 65.
- [47] J. W. Krumpfer, T. J. McCarthy, *Langmuir* **2011**, 27, 11514.
- [48] K. Glasmästar, J. Gold, A. S. Andersson, D. S. Sutherland, B. Kasemo, *Langmuir* **2003**, 19, 5475.
- [49] S. Yunus, C. de Crombrugge de Looinghe, C. Polenuis, A. Delcorte, *Surf. Interface Anal.* **2007**, 39, 922.
- [50] J. A. Wigenius, M. Hamed, O. Inganäs, *Adv. Funct. Mater.* **2008**, 18, 2563.
- [51] K. Ellinas, S. P. Pujari, D. A. Dragatogiannis, C. A. Charitidis, A. Tserepi, H. Zuilhof, E. Gogolides, *ACS Appl. Mater. Interfaces* **2014**, 6, 6510.
- [52] X. Li, B. Chen, W. Cai, T. Wang, Z. Wu, J. Li, *RSC Adv.* **2017**, 7, 11381.
- [53] B. Ruben, M. Elisa, L. Leandro, M. Victor, G. Gloria, S. Marina, S. M. K. R. Pandiyan, L. Nadhira, *Micro Nano Lett.* **2017**, 12, 754.
- [54] S. Xiong, L. Wan, Y. Ishida, Y.-A. Chapuis, G. S. W. Craig, R. Ruiz, P. F. Nealey, *ACS Nano* **2016**, 10, 7855.
- [55] C. C. Kathrein, W. Bai, J. A. Currihan-Incorvia, G. Lontos, K. Ntetsikas, A. Avgeropoulos, A. Böker, L. Tsarkova, C. A. Ross, *Chem. Mater.* **2015**, 27, 6890.
- [56] S. N. Magonov, M.-H. Whangbo, *Adv. Mater.* **1994**, 6, 355.
- [57] P. Kékicheff, C. Contal, *Langmuir* **2019**, 35, 3087.
- [58] C. A. Chavarin, A. A. Sagade, D. Neumaier, G. Bacher, W. Mertin, *Appl. Phys. A* **2016**, 122, 58.
- [59] M. Hafemeister, S. Siebentritt, J. Albert, M. C. Lux-Steiner, S. Sadewasser, *Phys. Rev. Lett.* **2010**, 104, 196602.
- [60] H. Hoppe, T. Glatzel, M. Niggemann, A. Hinsch, M. C. Lux-Steiner, N. S. Sariciftci, *Nano Lett.* **2005**, 5, 269.
- [61] W. Melitz, J. Shen, A. C. Kummel, S. Lee, *Surf. Sci. Rep.* **2011**, 66, 1.
- [62] R. Williams, *Phys. Rev.* **1965**, 140, A569.
- [63] C. B. Duke, W. R. Salaneck, T. J. Fabish, J. J. Ritsko, H. R. Thomas, A. Paton, *Phys. Rev. B* **1978**, 18, 5717.
- [64] C. Yun, S.-H. Lee, J. Ryu, K. Park, J.-W. Jang, J. Kwak, S. Hwang, *J. Am. Chem. Soc.* **2018**, 140, 14687.
- [65] X. Chen, I. I. Perepichka, C. G. Bazuin, *ACS Appl. Mater. Interfaces* **2014**, 6, 18360.
- [66] H. Xu, R. Hong, X. Wang, R. Arvizo, C. You, B. Samanta, D. Patra, M. T. Tuominen, V. M. Rotello, *Adv. Mater.* **2007**, 19, 1383.
- [67] K. Kim, H. Ryoo, K. S. Shin, *Langmuir* **2010**, 26, 10827.
- [68] W. Kern, *Proc. - Electrochem. Soc.* **1990**, 90, 3.
- [69] D. John, *Ph.D. Thesis*, University Potsdam (Potsdam, Germany) **2017**.
- [70] G. Frens, *Nature Phys. Sci.* **1973**, 241, 20.